Electronic Supplementary Material (ESI) for Journal of Materials Chemistry B.
This journal is © The Royal Society of Chemistry 2021

Supporting Information

Development and Demonstration of Functionalized Inorganic-Organic Hybrid Copper Phosphate Nanoflowers for Mimicking the Oxidative Reactions of Metalloenzymes by Working as a Nanozyme

Rahul Nag[a,b] and Chebrolu Pulla Rao*[,a]

[a]Department of Chemistry, Indian Institute of Technology Tirupati, Settipalli post, Tirupati–517506, Andhra Pradesh, India, E-mail: *cprao@iittp.ac.in*

[b]Department of Chemistry, Indian Institute of Technology Bombay, Powai, Mumbai – 400 076, India

Contents

S1. **Characterization of Compounds**:

S1.1. L_1: ^{1}H-NMR: (500 MHz, $CDCl_3$, δ ppm) : 7.89 (s, 2H, OH), 7.77 (m, 4H, phth-H), 7.55 (m, 4H, phth-H), 7.05 (d, 4H, Ar-H), 6.88 (d, 4H, Ar-H), 6.72 (t, 2H, Ar-H), 6.64 (t, 2H, Ar-H), 4.33 (d, 4H, Ar-CH_2-Ar), 4.15 (m, 8H, OCH_2CH_2), 3.39 (d, 4H, Ar-CH_2-Ar), 2.48 (t, 4H,N-CH_2). ^{13}C-NMR ($CDCl_3$, δ ppm): 149.3,146.1,144.7,142.6,140.4,132.8,132.6,132.2,130.7,130.5,129.2,129.1,128.9,128.5,123.5, 123.1,122.0,121.7,111.3,101.7. ESI-MS peak observed for $\mathbf{L_1}$ ($C_{19}H_{13}N_3$): Calcd.: 283.33; Found: 284.09 $[M+ H]^+$.

S1.2. **L_2**: ^{1}H-NMR: (500 MHz, $CDCl_3$, δ ppm) : 7.89 (s, 2H, OH), 7.77 (m, 4H, phth-H), 7.55 (m, 4H, phth-H), 7.05 (d, 4H, Ar-H), 6.88 (d, 4H, Ar-H), 6.72 (t, 2H, Ar-H), 6.64 (t, 2H, Ar-H), 4.33 (d, 4H, Ar-CH_2-Ar), 4.15 (m, 8H, OCH_2CH_2), 3.39 (d, 4H, Ar-CH_2-Ar), 2.48 (t, 4H,N-CH_2). ^{13}C-NMR ($CDCl_3$, δ ppm): 162.3,150.2,148.9,147.2,145.7,144.4,136.0,133.5,132.6,132.2,131.3,130.9,130.7,128.8,128.8, 127.8,126.4,125.6,125.5,124.3,123.5,123.2,111.4. ESI-MS peak observed for $\mathbf{L_2}$ ($C_{23}H_{15}N_3$): Calcd.: 333.39; Found: 334.1$[M+ H]^+$.

S1.3. **L_3**: ^{1}H-NMR: (500 MHz, $CDCl_3$, δ ppm) : 7.89 (s, 2H, OH), 7.77 (m, 4H, phth-H), 7.55 (m, 4H, phth-H), 7.05 (d, 4H, Ar-H), 6.88 (d, 4H, Ar-H), 6.72 (t, 2H, Ar-H), 6.64 (t, 2H, Ar-H), 4.33 (d, 4H, Ar-CH_2-Ar), 4.15 (m, 8H, OCH_2CH_2), 3.39 (d, 4H, Ar-CH_2-Ar), 2.48 (t, 4H,N-CH_2). ^{13}C-NMR ($CDCl_3$, δ ppm): 173.4,161.8,150.3,149.0,147.4,145.7,144.6,136.2,132.2,131.6,130.8,130.5,129.1,128.9,127.9, 126.3,125.7,125.6,124.8,123.5,123.4,111.7. ESI-MS peak observed for $\mathbf{L_3}$ ($C_{27}H_{17}N_3$): Calcd.: 383.44; Found: 384.15$[M+ H]^+$.

S1.4. **L_4**: ^{1}H-NMR: (500 MHz, $CDCl_3$, δ ppm) : 7.89 (s, 2H, OH), 7.77 (m, 4H, phth-H), 7.55 (m, 4H, phth-H), 7.05 (d, 4H, Ar-H), 6.88 (d, 4H, Ar-H), 6.72 (t, 2H, Ar-H), 6.64 (t, 2H, Ar-

H), 4.33 (d, 4H, Ar-CH_2-Ar), 4.15 (m, 8H, OCH_2CH_2), 3.39 (d, 4H, Ar-CH_2-Ar), 2.48 (t, 4H,N-CH_2). ^{13}C-NMR ($CDCl_3$, δ ppm):

161.3,150.7,149.3,147.6,146.0,144.7,136.8,133.8,133.0,131.2,130.9,130.5,129.9,129.8,129.4, 128.5,127.9,127.7,127.2,127.0,126.7,126.4,125.7,124.,124.,123.,123.3,112.1. ESI-MS peak observed for **L_4** ($C_{29}H_{17}N_3$): Calcd.: 407.47; Found: 408.15[M+ H]$^+$.

S2. Spectra of $\mathbf{L_1}$.

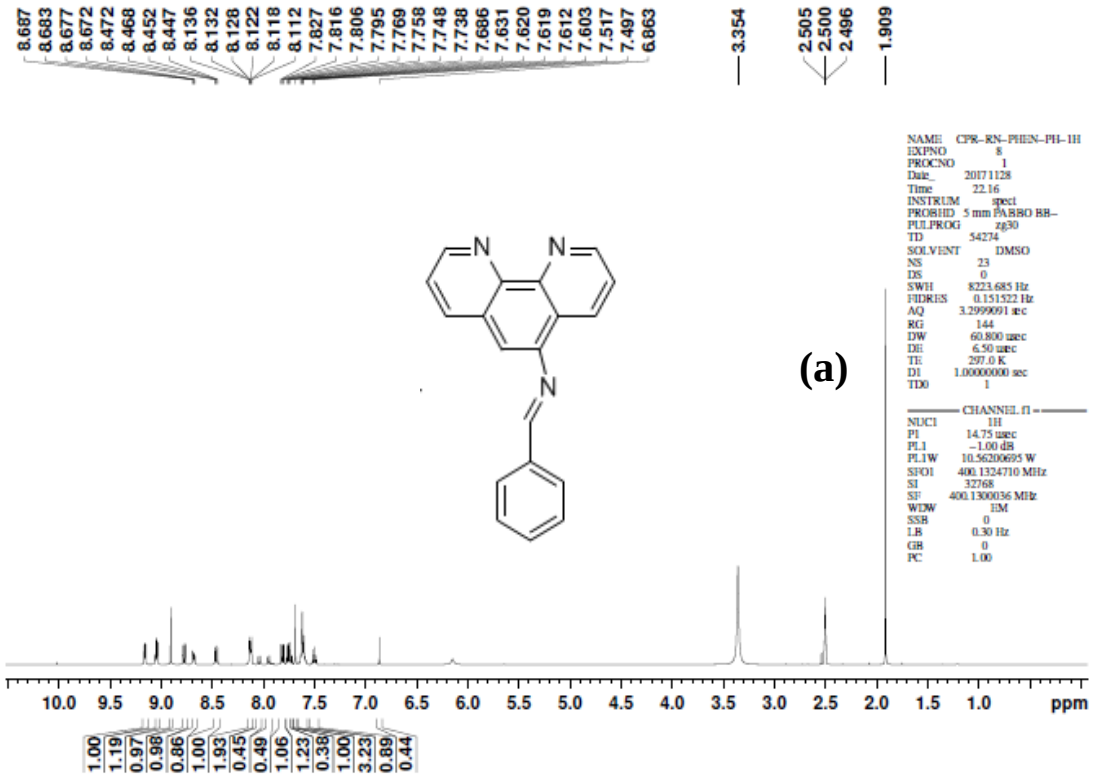

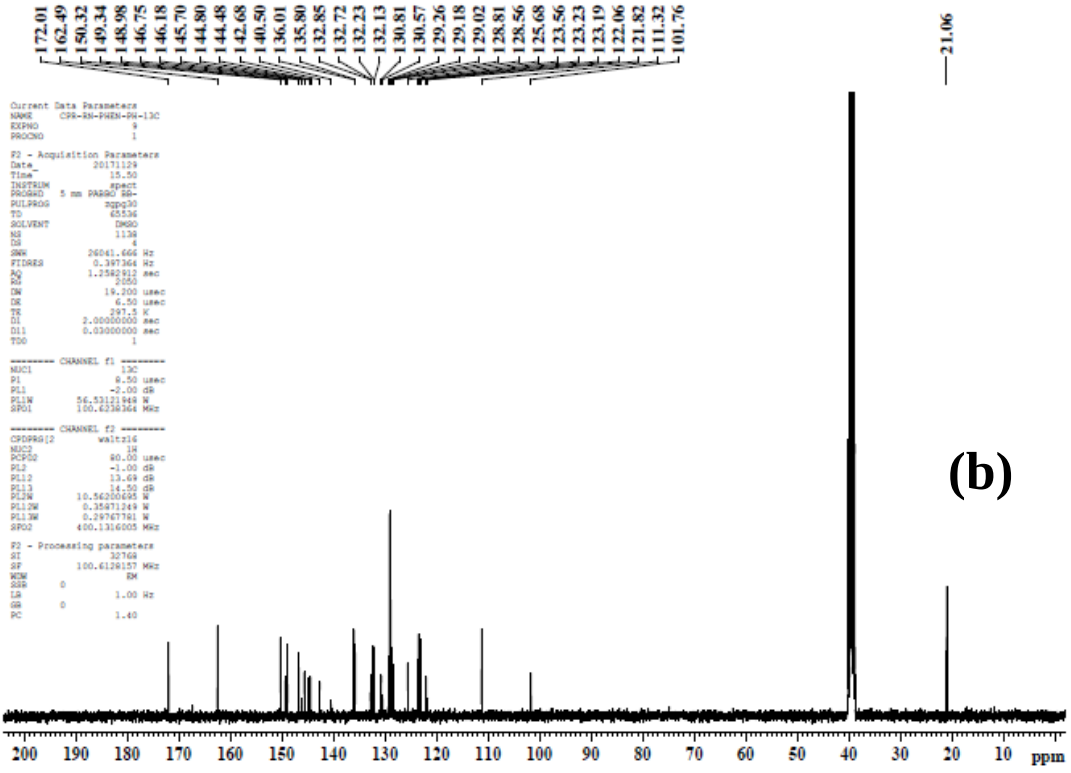

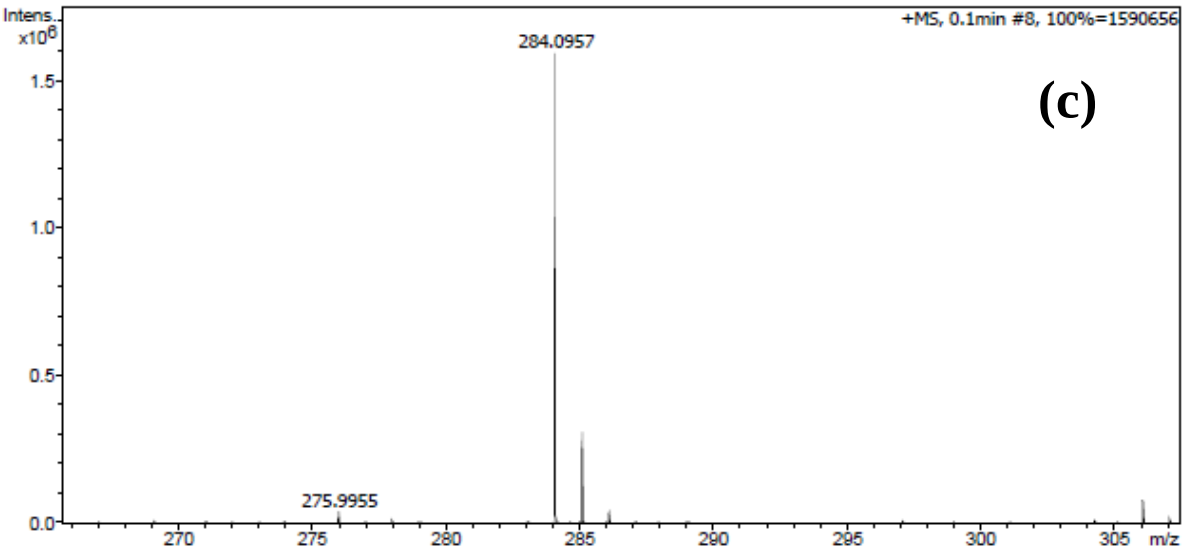

Fig. S01 (a) ^{1}H, (b) ^{13}C NMR spectra of $\mathbf{P_1}$ in $CDCl_3$ and (c) ESI-MS spectrum of $\mathbf{L_1}$.

S3. Spectra of $\mathbf{L_2}$.

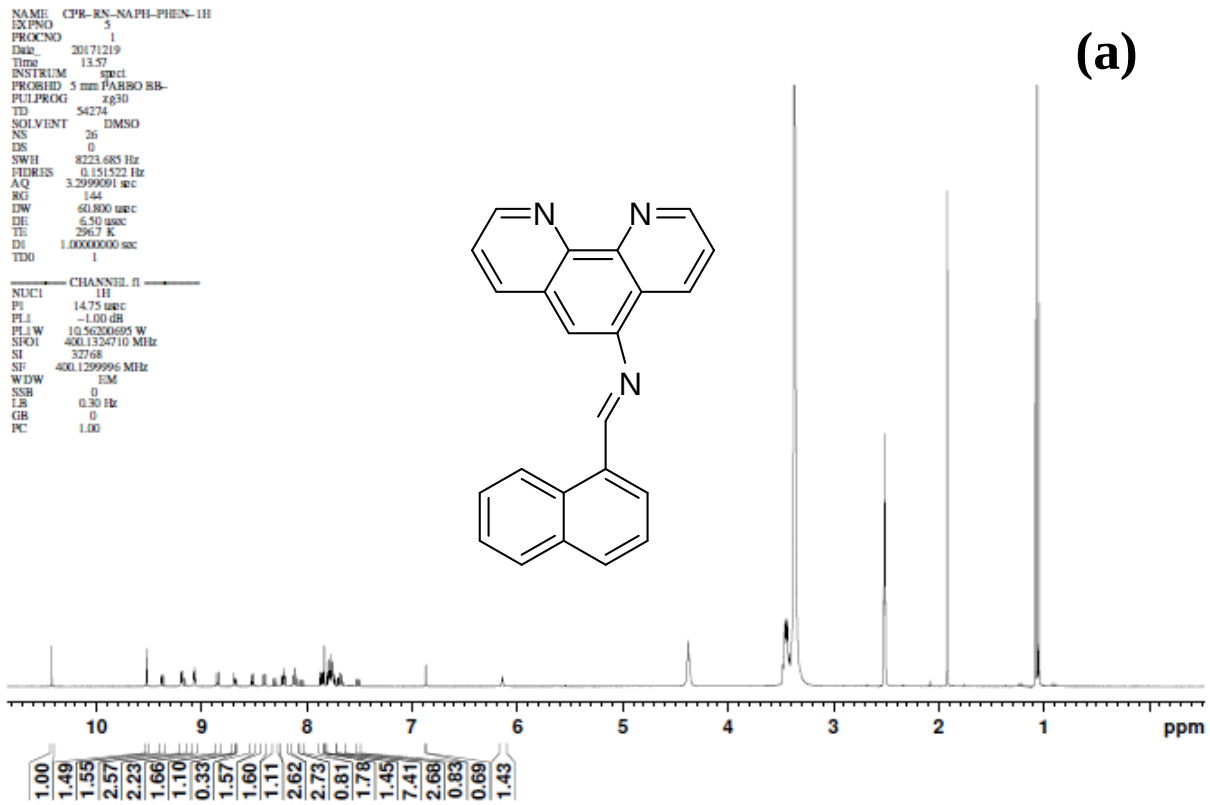

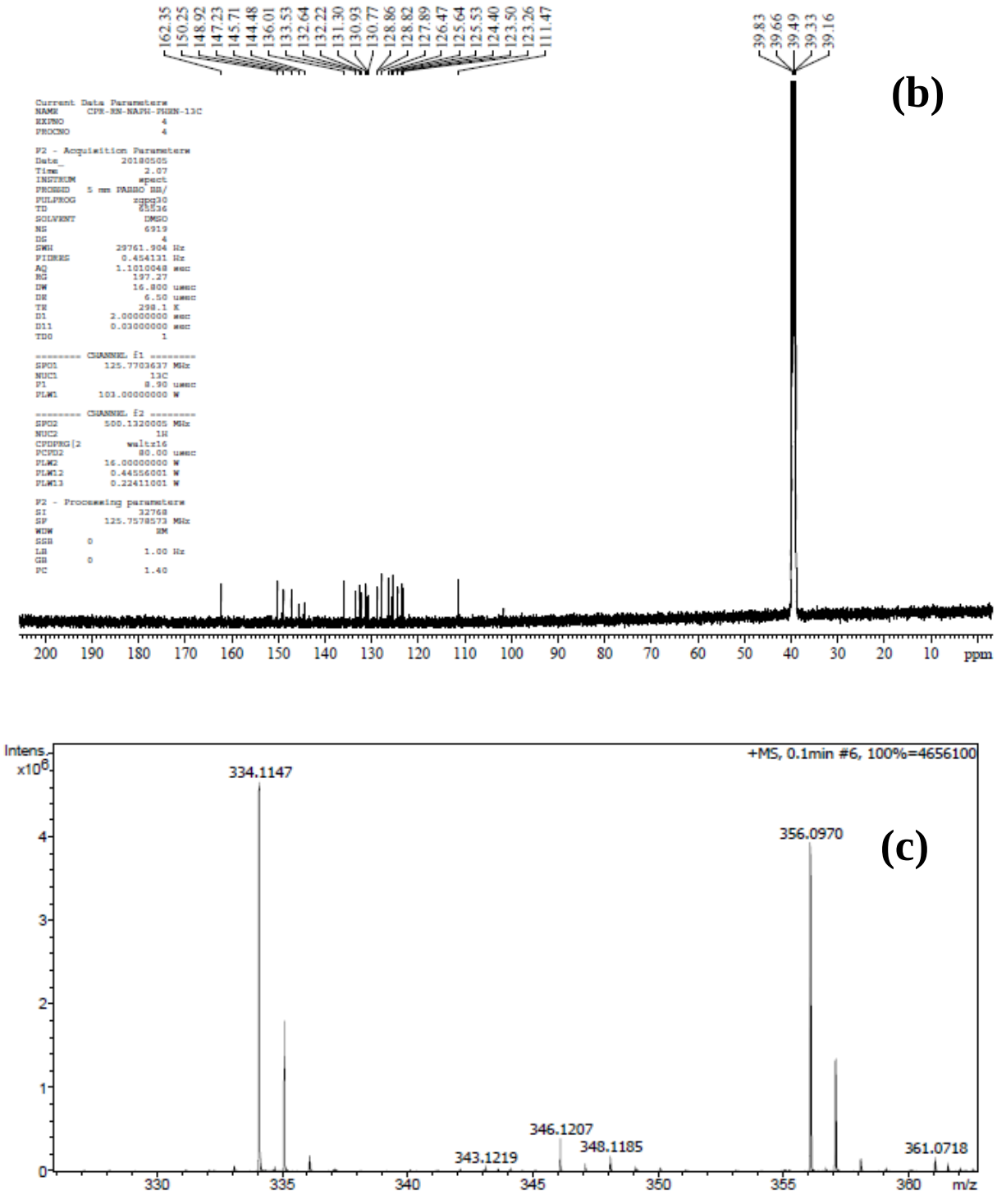

Fig. S02 (a) ^{1}H, (b) ^{13}C NMR spectra of **L_2** in DMSO-D_6 and (c) ESI-MS spectrum of **L_2**.

S4. Spectra for $\mathbf{L_3}$:

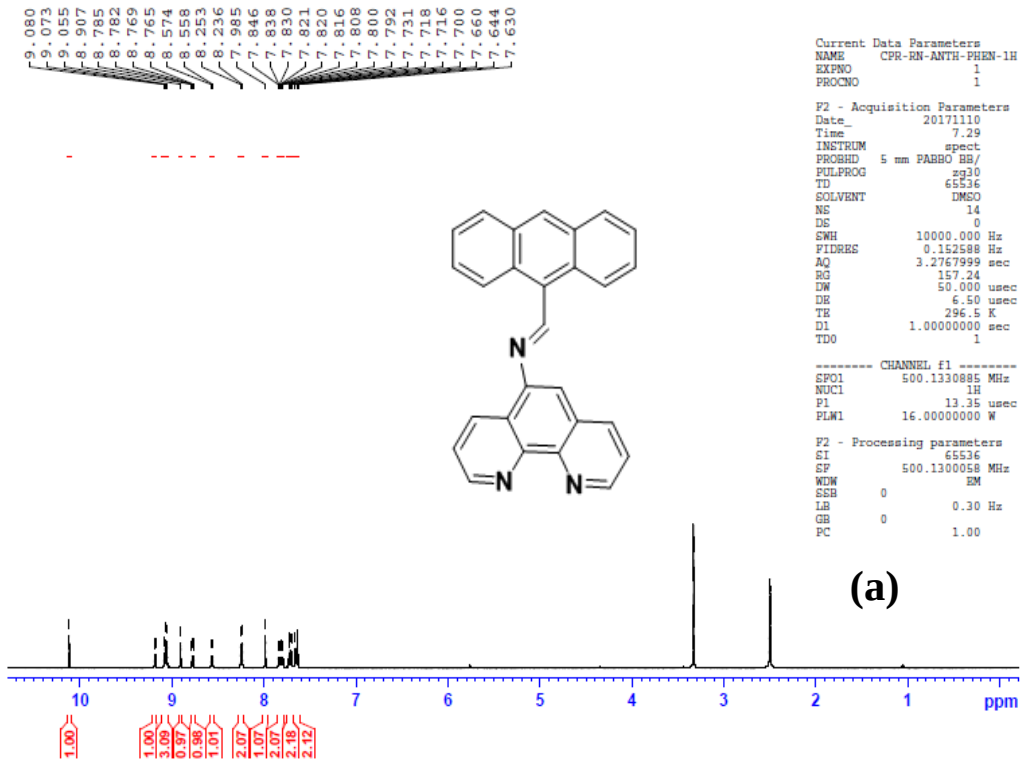

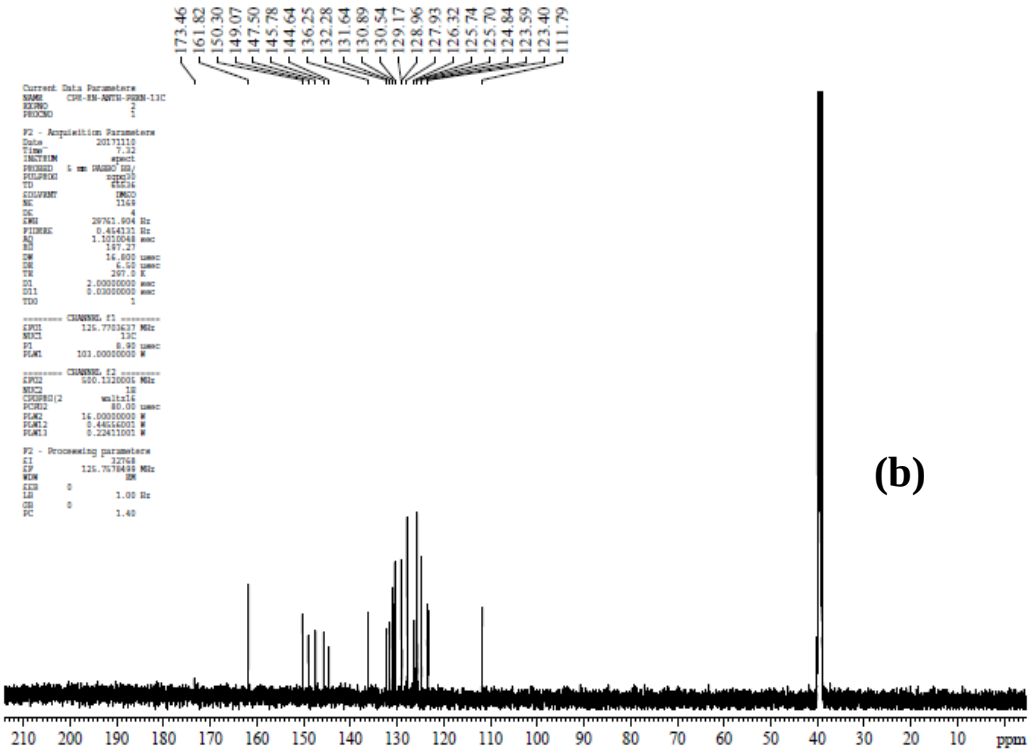

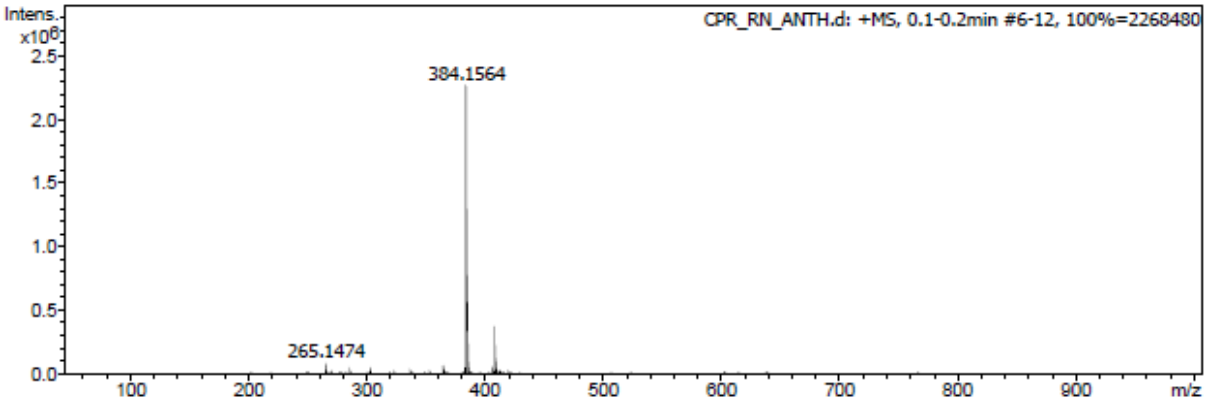

Fig. S03 (a) ^{1}H, (b) ^{13}C NMR spectra of $\mathbf{L_3}$ in DMSO-D_6 and (c) ESI-MS spectrum of $\mathbf{L_3}$.

S5 Spectra for **L_4**:

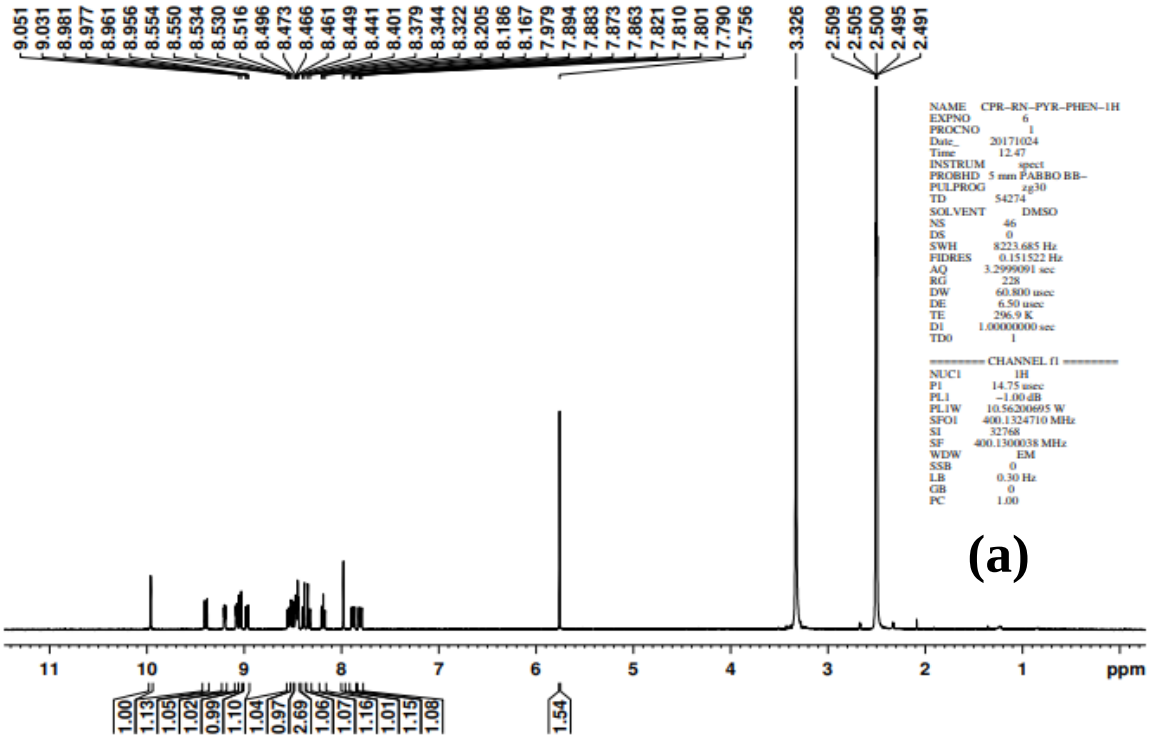

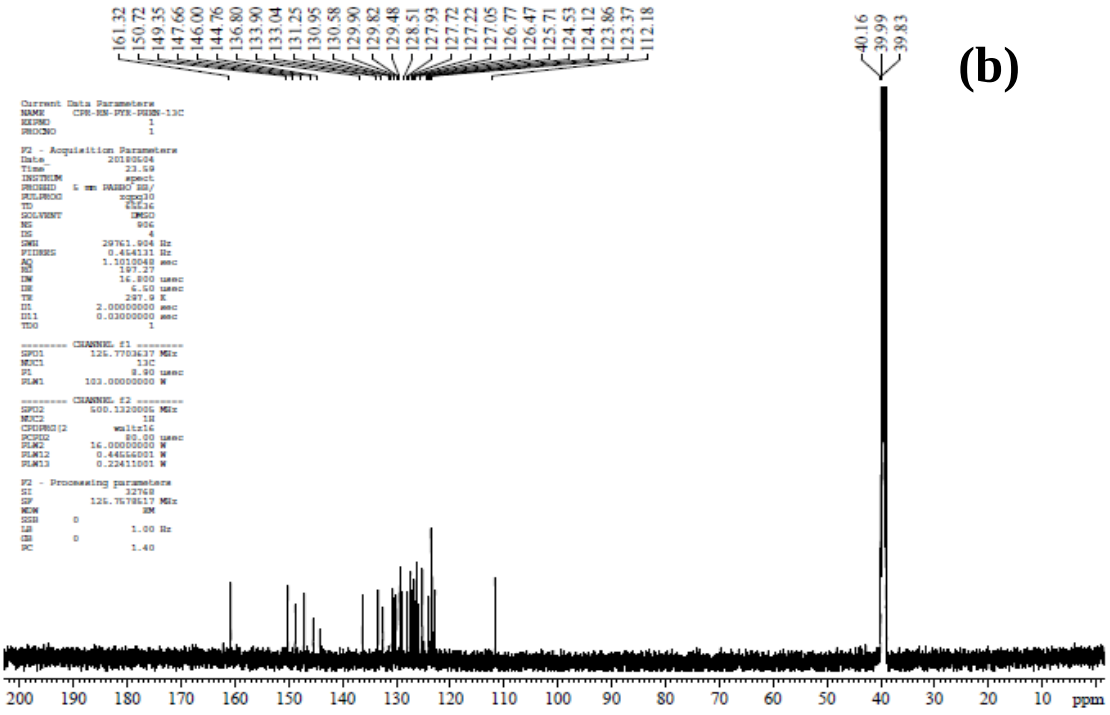

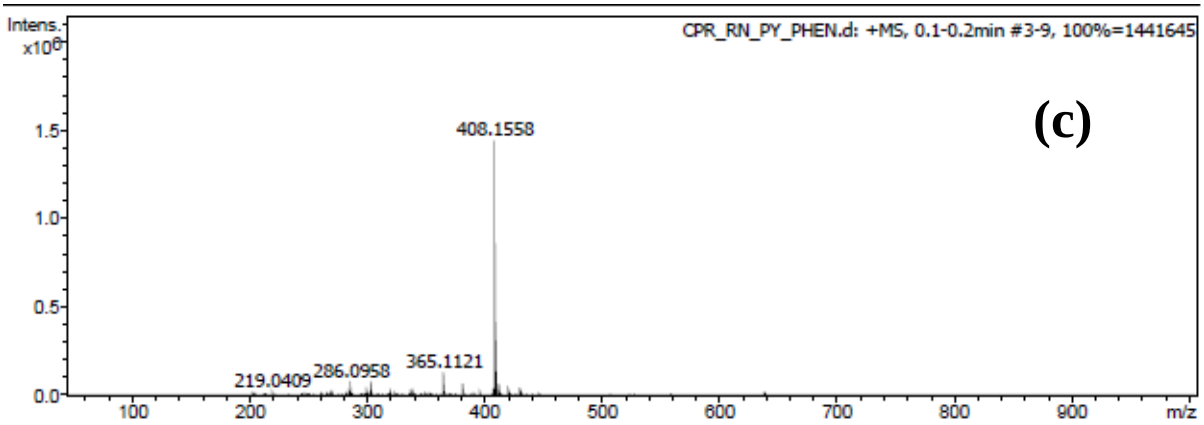

Fig. S04 (a) ^{1}H, (b) ^{13}C NMR spectra of $\mathbf{L_4}$ in DMSO-D_6 and (c) ESI-MS spectrum of $\mathbf{L_4}$.

S6. FT-IR spectra for CuPNF and $\mathbf{L_n}$-CuPNF.

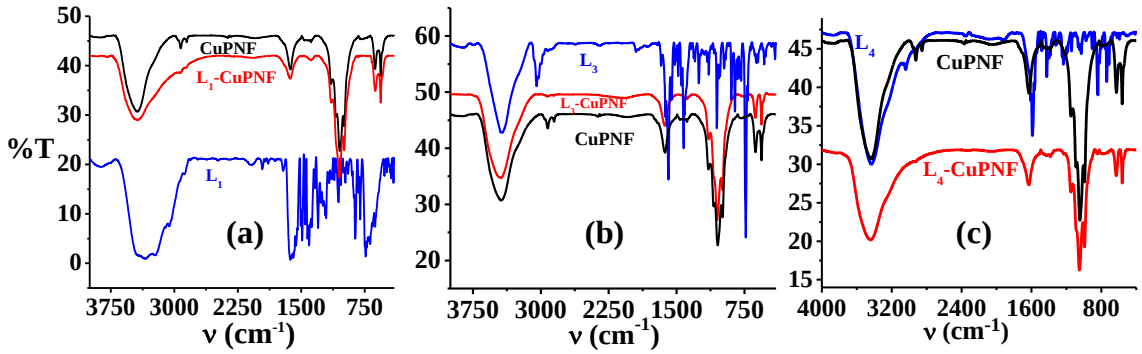

Fig. S05 FT-IR spectra for CuPNF and (a) $\mathbf{L_1}$-CuPNF, (b) $\mathbf{L_3}$-CuPNF and (c) $\mathbf{L_4}$-CuPNF.

S7. XPS spectra for **L_4**-CuPNFs.

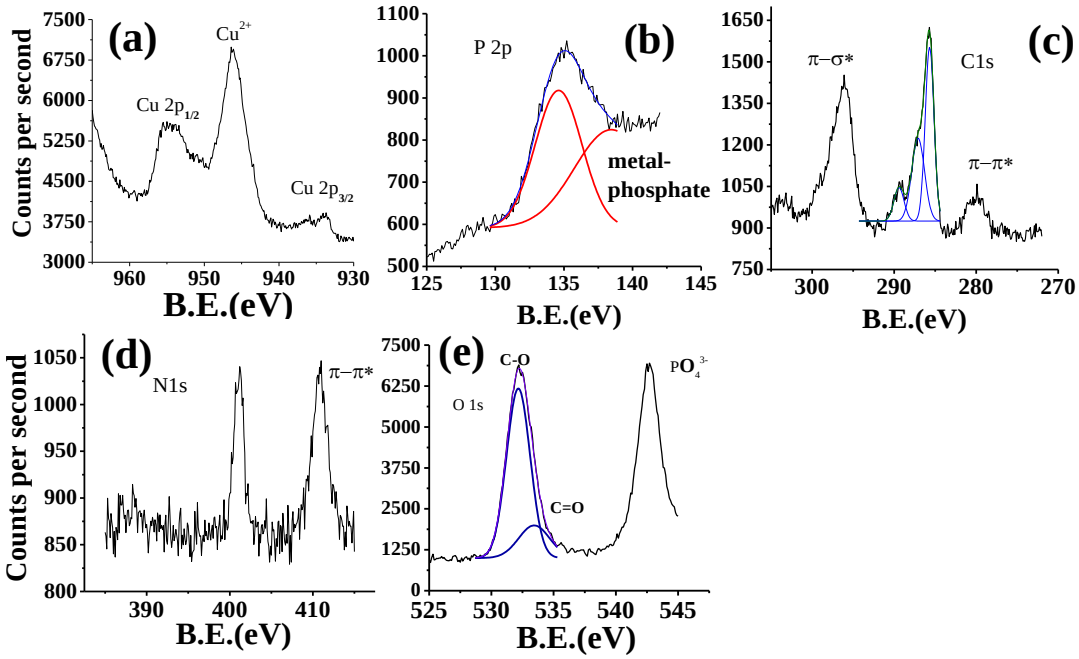

Fig. S06 XPS spectra for (a) Cu 2p, (b) P 2p, (c) C 1s, (d) N 1s and (e) O 1s of **L_4**-CuPNFs.

S8. Petal Morphology for Hybrid Nanoflowers.

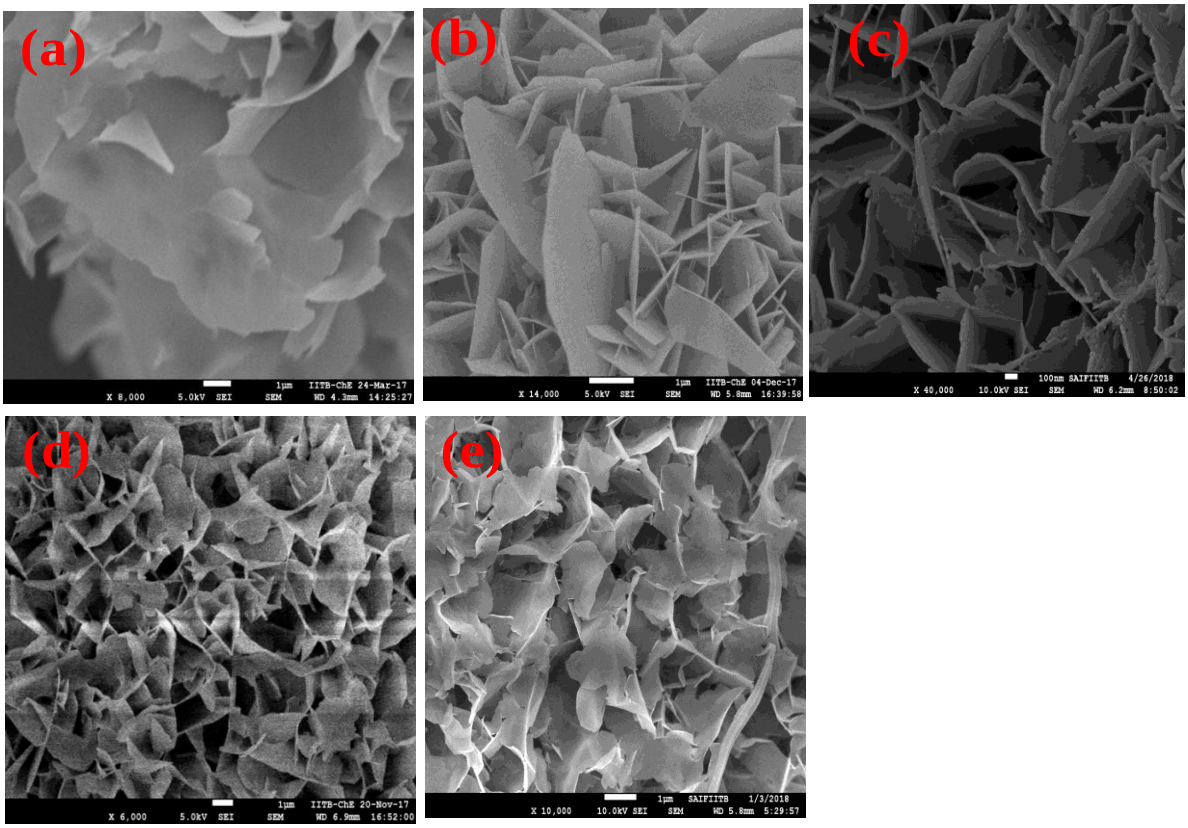

Fig. S07 FEG-SEM micrographs of (a) **CuPNF** (Scale bare: 1 μm), (b) **L_1**-CuPNF (Scale bare: 1 μm), (c) **L_2**-CuPNF (Scale bare: 100 nm), (d) **L_3**-CuPNF (Scale bare: 1 μm), (e) **L_4**-CuPNF (Scale bare: 1 μm).

S9. Size Distribution of Hybrid Nanoflowers.

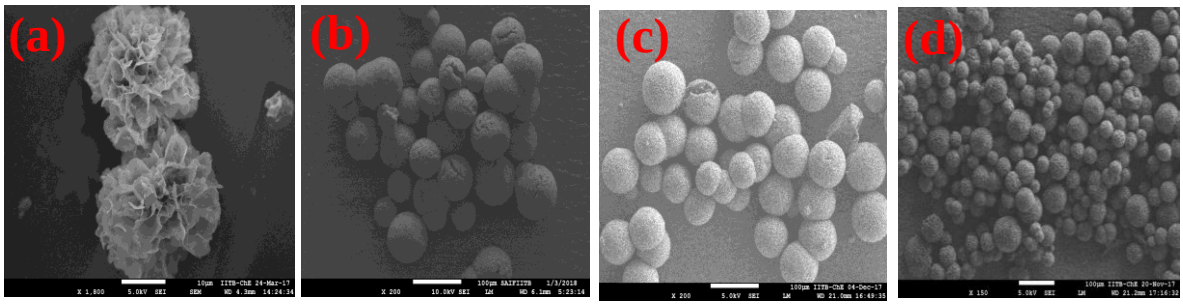

Fig. S08 Size distribution from SEM of (a) **L_1**-CuPNF (Scale bare: 10 μm), (b) **L_2**-CuPNF (Scale bare: 100 μm), (c) **L_3**-CuPNF (Scale bare: 100 μm), (d) **L_4**-CuPNF (Scale bare: 100 μm).

S10. Nanoflower Growth upon Varying [Cu^{2+}].

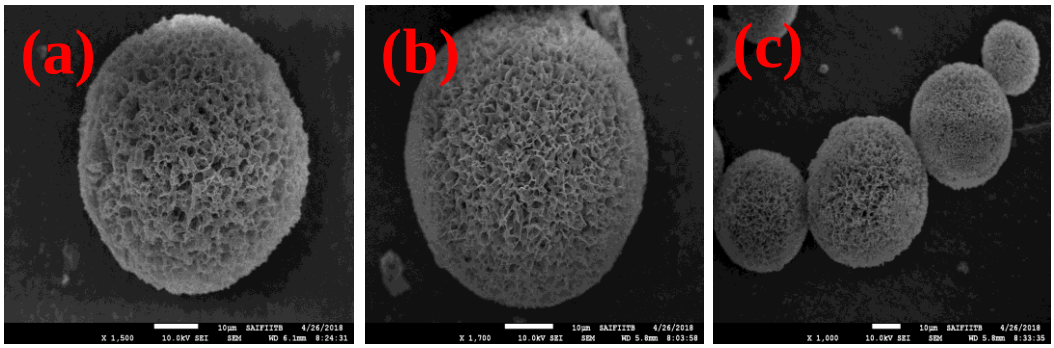

Fig. S09 SEM micrographs of $\mathbf{L_4}$-CuPNF while varying Cu^{2+} concentration: (a) 80 mM, (b) 120 mM, (c) 200 mM. (Scale bare: 10 μm for (a), (b) and (c)).

S11. FEG-SEM Micrographs Showing Petal Thickness.

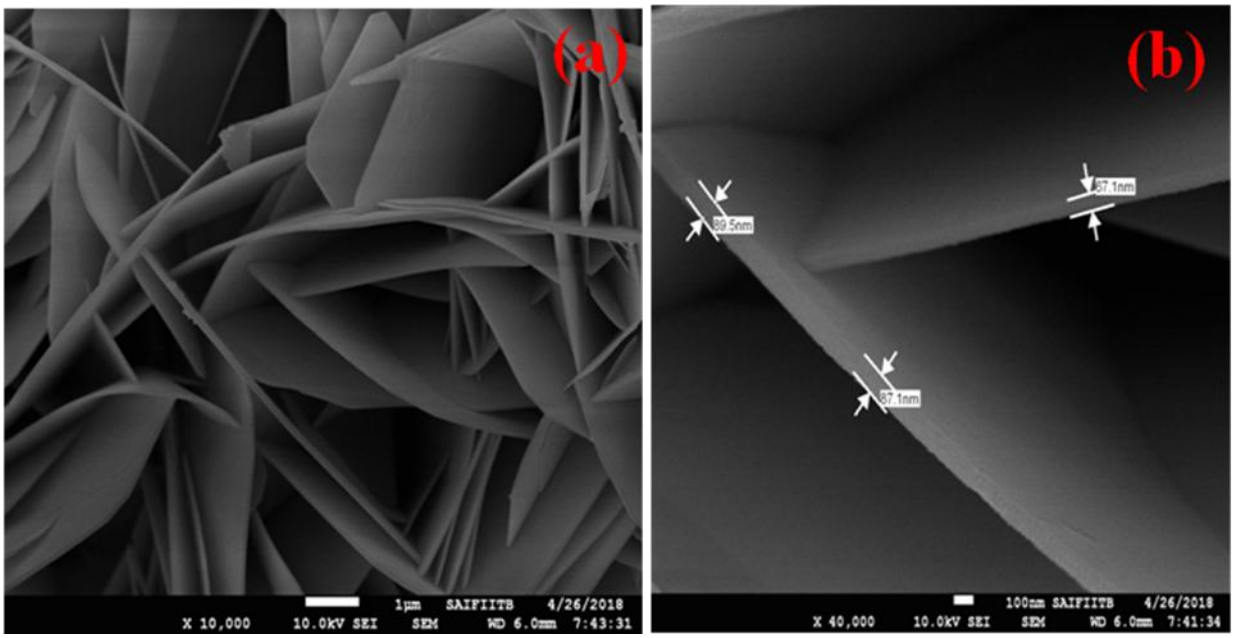

Fig. S10 HR-SEM image of (a) $\mathbf{L_4}$-CuPNF (Scale bare: 1 μm) and its (b) enlarged view (Scale bare: 100 nm).

S12. EDS spectra for **L_4**-CuPNF.

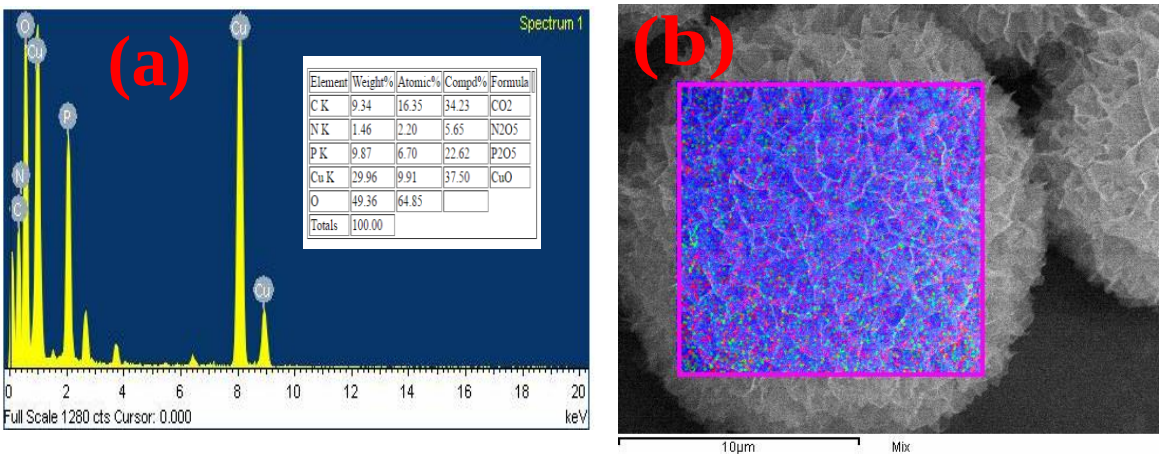

Fig. S11 EDS analysis from SEM micrographs of (a) and (b) for **L_4**-CuPNF.

S13. A Schematic Diagram for the Formation of $\mathbf{L_n}$-CuPNFs.

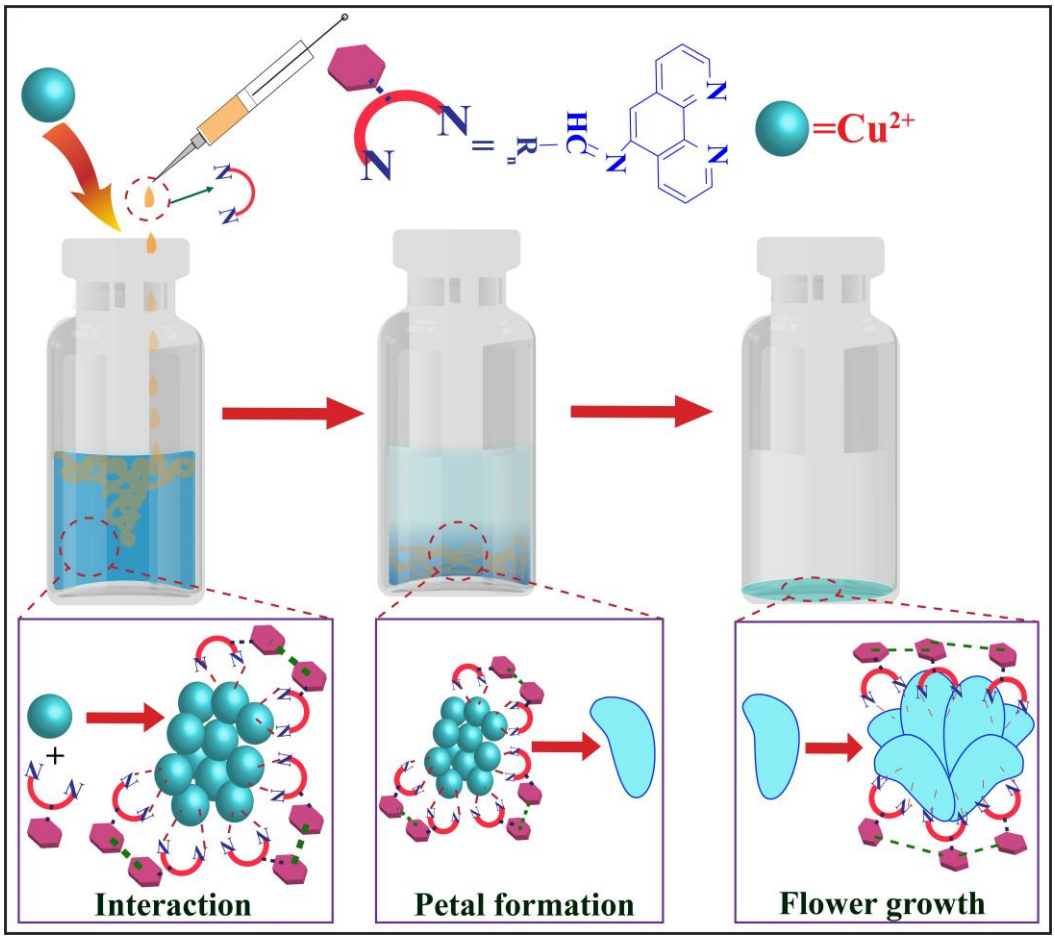

Fig. S12 Schematic representation for the formation and growth of the nanoflower in the presence of $\mathbf{L_n}$ conjugates.

S14. Absorption Data for OPD Oxidation.

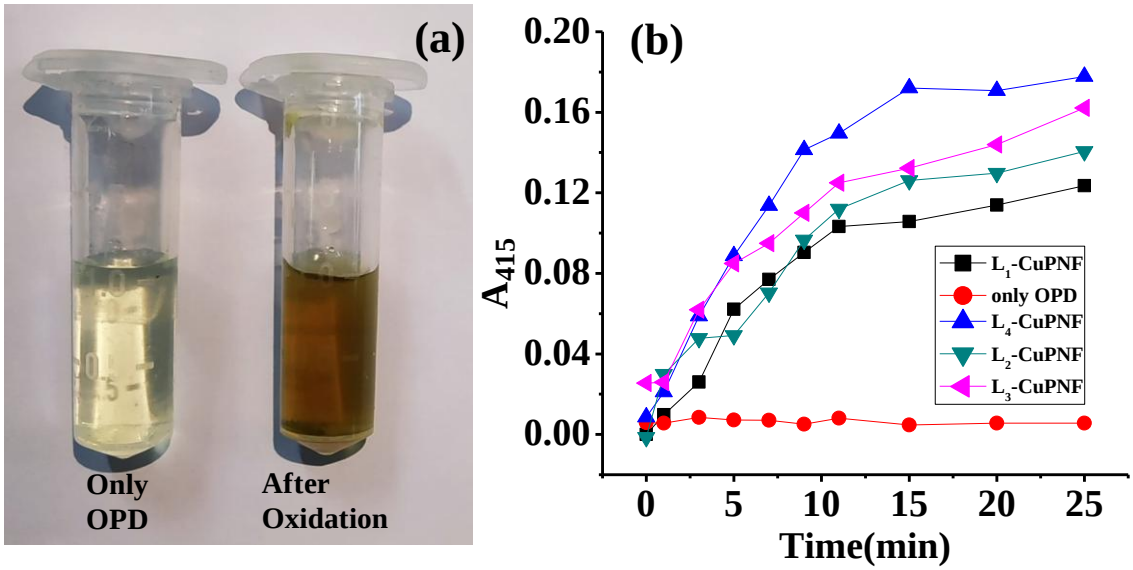

Fig. S13 (a) Colorimetric changes showing OPD oxidation in the presence of **L_4**-CuPNF/H_2O_2. (b) A_{415} vs time plot for OPD Oxidation to 2,3-diaminophenazine (DAP, λ_{max}=415 nm) in the presence of **L_n**-CuPNFs. (OPD=5 mM, H_2O_2=50 mM, PBS buffer (pH 7.4 10 mM), **L_n**-CuPNFs=1 mg/mL).

S15. Concentration Optimization and Study of the Mechanism of Peroxidase Activity.

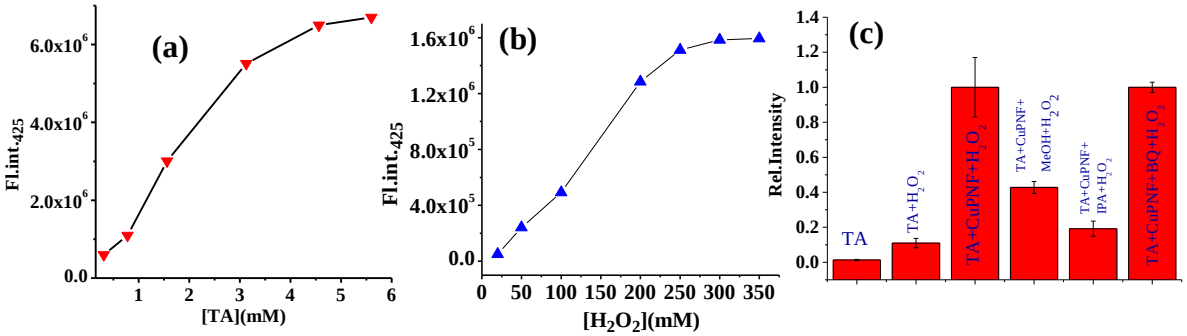

Fig. S14 TA oxidation in presence of **L_4**-CuPNFs (1 mg/mL) (a) keeping [H_2O_2] constant at 150 mM varying [TA] and (b) keeping [TA] constant at 0.8 mM varying [H_2O_2] in phosphate buffer (pH 7.0) shown via plotting fluorescence intensity at 425 nm *vs.* respective concentrations of the substrates (TA/H_2O_2). (c) Relative intensity plot at 425 nm showing TA oxidation in presence hydroxyl (methanol and isopropanol=1 mg/mL) and superoxide radical trap (benzoquinone=1 mg/mL) and CuPNFs/H_2O_2.

S16. Absorption data for Ascorbate Oxidation.

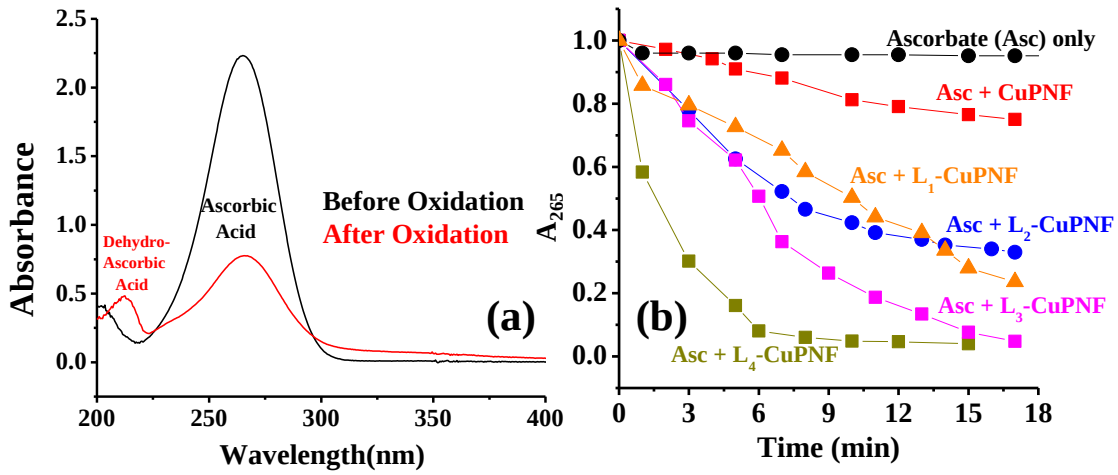

Fig. S15 (a) Absorption spectra for the ascorbate and dehydroascorbate. (b) Relative absorbance data for Ascorbate Oxidation in the presence of CuPNF and **L$_n$**-CuPNFs (sodium ascorbate= 50µM, phosphate buffer (pH= 7.0, 5 mM), **L$_n$**-CuPNF= 100 µg/mL).

S17. Absorption Data for Dopamine Oxidase Study.

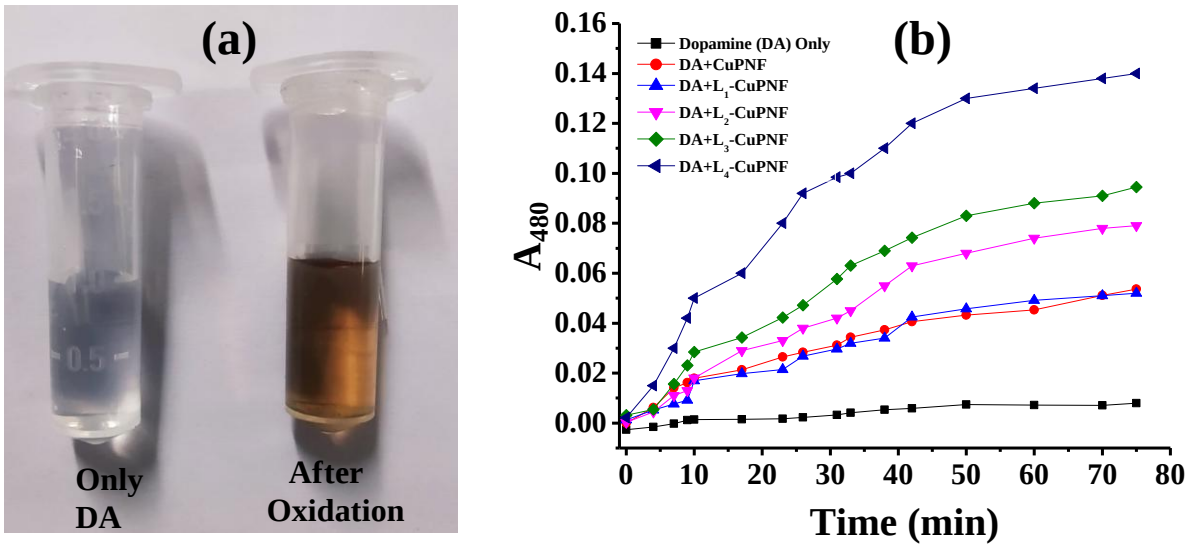

Fig. S16 (a) Colorimetric changes showing DA oxidation in the presence of **L$_4$**-CuPNFs. (b) A_{480} *vs.* time plot for dopamine oxidation to aminochrome in the presence of CuPNF and **L$_n$**-CuPNFs (dopamine= 10 µM, PBS buffer (pH= 7.4, 10 mM), **L$_n$**-CuPNF= 100 µg/mL).

S18. ESI-MS Spectrum for the Copper Complex of $\mathbf{L_4}$.

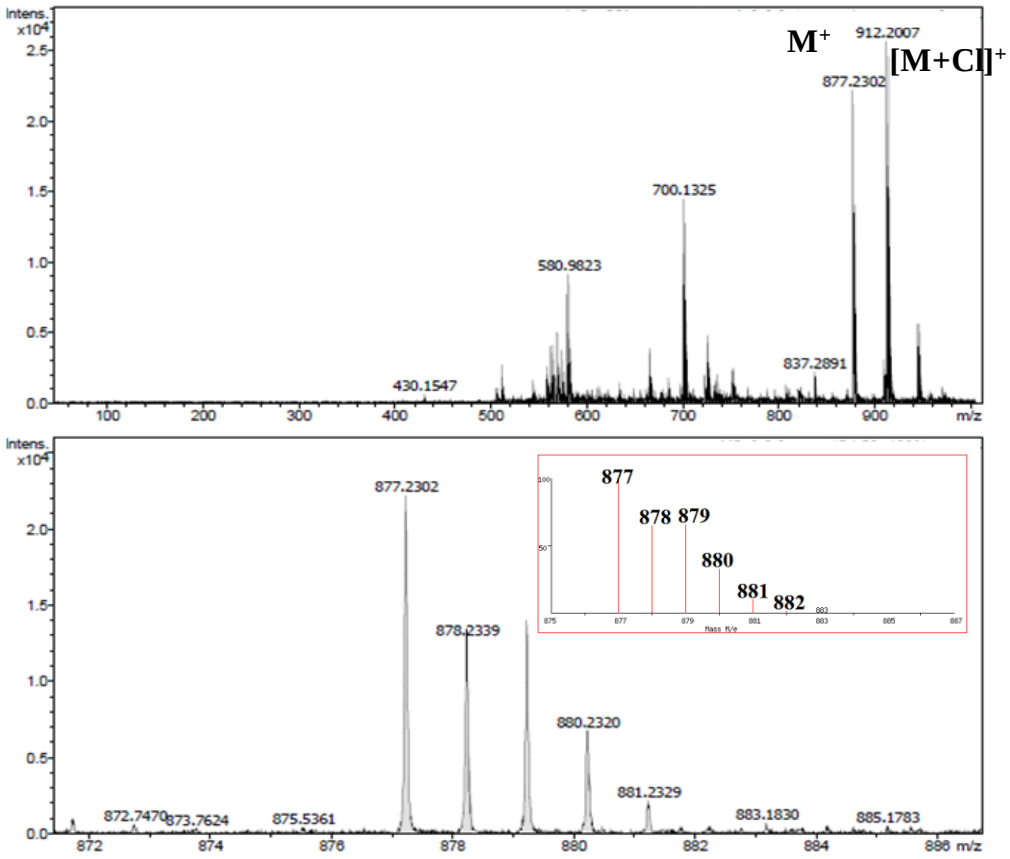

Fig. S17 ESI-MS spectrum for the copper complex of $\mathbf{L_4}$. The experimental and calculated isotopic peak pattern has been given for comparison.

S19. Characterization of the Copper Complex of $\mathbf{L_4}$.

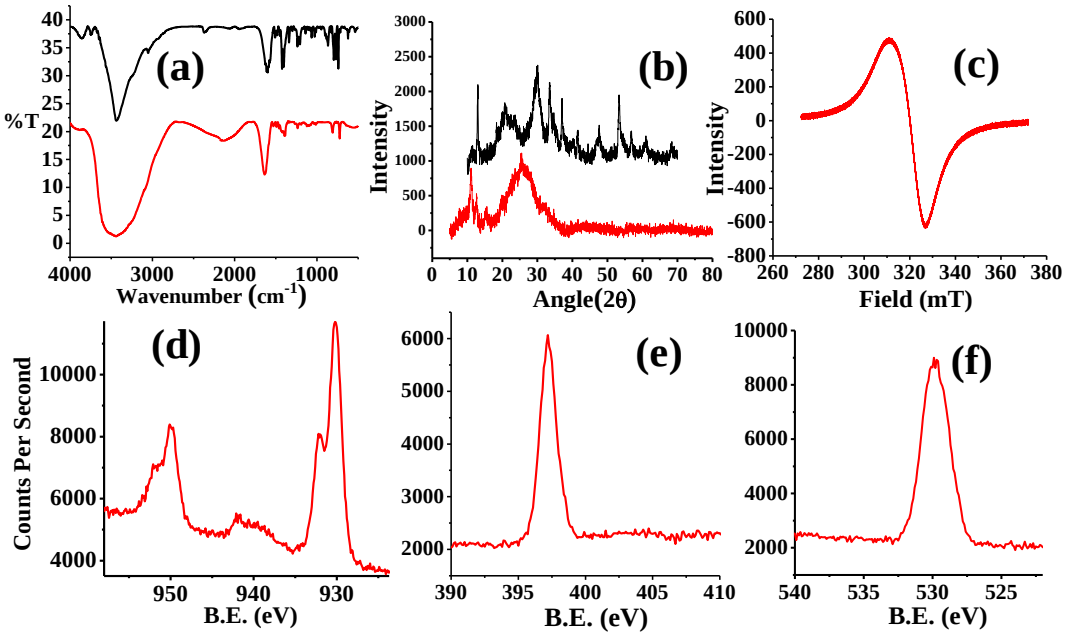

Fig. S18 (a) FTIR spectrum for $\mathbf{L_4}$ (black) and Cu($\mathbf{L_4}$)$_2$ (red). (b) XRD spectrum for CuPNF-$\mathbf{L_4}$ and (black) and Cu($\mathbf{L_4}$)$_2$ (red). (c) EPR spectrum for Cu($\mathbf{L_4}$)$_2$. XPS spectrum for Cu($\mathbf{L_4}$)$_2$: (d) Cu 2p, (e) N 1s and (f) O 1s.

S20. Table S1. Copper Based Nanomaterials Possessing Peroxidase Mimetic Activity.

Natural Enzyme	**Nanomaterial**	**Applications**	**Reference**
Horse Radish Peroxidase	CuO	phenol degradation detection	*J. Environ. Sci. Technol.*, 2015, **12**, 653−660; *Biosens. Bioelectron.*, 2014, **61**, 374–378
	CuO/Pt	detection	*Analyst*, 2017, **142**, 2500−2506
	BSA-$Cu_3(PO_4)_2$	immunodetection	*Anal. Chem.*, 2008, **80**, 2250−2254
	Cu^{2+}-C-dots	detection	*ACS Nano*, 2017, **11**,3247−3253
	Cu^{2+}-g-C_3N_4	detection	
	Cu^{2+}-GO	detection	*Nano Lett.*, 2017, **17**, 2043−2048
	$CuInS_2$	detection	*Sens. Actuators B*, 2015, **209**, 670−676
	Cu NPs@C	detection	*Chem. Eur. J.*, 2014, **20**, 16377−16383
	CuS	immunodetection	*Anal. Methods*, 2015, **7**, 5454−5461; *ACS Appl. Mater. Interfaces*, 2016, **8**, 12031−12038
	$Cu(OH)_2$		*J. Am. Chem. Soc.*, 2015, **137**, 13957−13963
	$Cu_2(OH)_3Cl$-CeO_2	detection	*Microchim. Acta*, 2015, **182**, 1733−1738
	Cu-MOF	detection	*Anal. Chim. Acta*, 2015, **856**, 90−95; *Anal. Chim. Acta*, 2018, **1004**, 74−81
	Cu-β-LG	detection	*ACS Appl. Mater. Interfaces*, 2016, **8**,10392–10402
	Asn/Lys-$Cu_3(PO_4)_2$	Dye Degradation	*Sci. Rep.*, 2016, **6**, 22412
	GO_x&HRP–$Cu_3(PO_4)_2 \cdot 3H_2O$	Glucose Detection	*Nanoscale*, 2014, **6**, 255–262
	HRP-$Cu_3(PO_4)_2$ from copper foil	Colorimetric TMB oxidation	*Colloids and Surfaces B: Biointerfaces*, 2015, **135**, 613–618

	L_n- $Cu_3(PO_4)_2$ (L_n = aromatic [phenyl, naphthyl, anthracenyl, pyrenyl] phenanthroline conjugates)	**<u>potential applications</u>: detection, water purification**	**Present Work**